BABAR-PUB-15/008
SLAC-PUB-16422

arXiv:1511.02310v3 [hep-ex] 4 Jan 2016

Measurement of the $I = 1/2$ $K\pi$ $\mathcal{S}$-wave amplitude from Dalitz plot analyses of $\eta_c \to K\overline{K}\pi$ in two-photon interactions

J. P. Lees, V. Poireau, and V. Tisserand
Laboratoire d'Annecy-le-Vieux de Physique des Particules (LAPP), Université de Savoie, CNRS/IN2P3, F-74941 Annecy-Le-Vieux, France

E. Grauges
Universitat de Barcelona, Facultat de Fisica, Departament ECM, E-08028 Barcelona, Spain

A. Palano*
INFN Sezione di Bari and Dipartimento di Fisica, Università di Bari, I-70126 Bari, Italy

G. Eigen
University of Bergen, Institute of Physics, N-5007 Bergen, Norway

D. N. Brown and Yu. G. Kolomensky
Lawrence Berkeley National Laboratory and University of California, Berkeley, California 94720, USA

H. Koch and T. Schroeder
Ruhr Universität Bochum, Institut für Experimentalphysik 1, D-44780 Bochum, Germany

C. Hearty, T. S. Mattison, J. A. McKenna, and R. Y. So
University of British Columbia, Vancouver, British Columbia, Canada V6T 1Z1

V. E. Blinov[abc], A. R. Buzykaev[a], V. P. Druzhinin[ab], V. B. Golubev[ab], E. A. Kravchenko[ab], A. P. Onuchin[abc], S. I. Serednyakov[ab], Yu. I. Skovpen[ab], E. P. Solodov[ab], and K. Yu. Todyshev[ab]
Budker Institute of Nuclear Physics SB RAS, Novosibirsk 630090[a], Novosibirsk State University, Novosibirsk 630090[b], Novosibirsk State Technical University, Novosibirsk 630092[c], Russia

A. J. Lankford
University of California at Irvine, Irvine, California 92697, USA

J. W. Gary and O. Long
University of California at Riverside, Riverside, California 92521, USA

A. M. Eisner, W. S. Lockman, and W. Panduro Vazquez
University of California at Santa Cruz, Institute for Particle Physics, Santa Cruz, California 95064, USA

D. S. Chao, C. H. Cheng, B. Echenard, K. T. Flood, D. G. Hitlin, J. Kim, T. S. Miyashita, P. Ongmongkolkul, F. C. Porter, and M. Röhrken
California Institute of Technology, Pasadena, California 91125, USA

Z. Huard, B. T. Meadows, B. G. Pushpawela, M. D. Sokoloff, and L. Sun
University of Cincinnati, Cincinnati, Ohio 45221, USA

J. G. Smith and S. R. Wagner
University of Colorado, Boulder, Colorado 80309, USA

D. Bernard and M. Verderi
Laboratoire Leprince-Ringuet, Ecole Polytechnique, CNRS/IN2P3, F-91128 Palaiseau, France

D. Bettoni[a], C. Bozzi[a], R. Calabrese[ab], G. Cibinetto[ab], E. Fioravanti[ab], I. Garzia[ab], E. Luppi[ab], and V. Santoro[a]

INFN Sezione di Ferrara[a]; Dipartimento di Fisica e Scienze della Terra, Università di Ferrara[b], I-44122 Ferrara, Italy

A. Calcaterra, R. de Sangro, G. Finocchiaro, S. Martellotti, P. Patteri, I. M. Peruzzi, M. Piccolo, and A. Zallo
INFN Laboratori Nazionali di Frascati, I-00044 Frascati, Italy

S. Passaggio and C. Patrignani[†]
INFN Sezione di Genova, I-16146 Genova, Italy

B. Bhuyan
Indian Institute of Technology Guwahati, Guwahati, Assam, 781 039, India

U. Mallik
University of Iowa, Iowa City, Iowa 52242, USA

C. Chen, J. Cochran, and S. Prell
Iowa State University, Ames, Iowa 50011, USA

H. Ahmed
Physics Department, Jazan University, Jazan 22822, Kingdom of Saudi Arabia

M. R. Pennington
Thomas Jefferson National Accelerator Facility, Newport News, Virginia 23606, USA

A. V. Gritsan
Johns Hopkins University, Baltimore, Maryland 21218, USA

N. Arnaud, M. Davier, F. Le Diberder, A. M. Lutz, and G. Wormser
Laboratoire de l'Accélérateur Linéaire, IN2P3/CNRS et Université Paris-Sud 11, Centre Scientifique d'Orsay, F-91898 Orsay Cedex, France

D. J. Lange and D. M. Wright
Lawrence Livermore National Laboratory, Livermore, California 94550, USA

J. P. Coleman, E. Gabathuler, D. E. Hutchcroft, D. J. Payne, and C. Touramanis
University of Liverpool, Liverpool L69 7ZE, United Kingdom

A. J. Bevan, F. Di Lodovico, and R. Sacco
Queen Mary, University of London, London, E1 4NS, United Kingdom

G. Cowan
University of London, Royal Holloway and Bedford New College, Egham, Surrey TW20 0EX, United Kingdom

Sw. Banerjee, D. N. Brown, and C. L. Davis
University of Louisville, Louisville, Kentucky 40292, USA

A. G. Denig, M. Fritsch, W. Gradl, K. Griessinger, A. Hafner, and K. R. Schubert
Johannes Gutenberg-Universität Mainz, Institut für Kernphysik, D-55099 Mainz, Germany

R. J. Barlow[‡] and G. D. Lafferty
University of Manchester, Manchester M13 9PL, United Kingdom

R. Cenci, A. Jawahery, and D. A. Roberts
University of Maryland, College Park, Maryland 20742, USA

R. Cowan
Massachusetts Institute of Technology, Laboratory for Nuclear Science, Cambridge, Massachusetts 02139, USA

R. Cheaib and S. H. Robertson

McGill University, Montréal, Québec, Canada H3A 2T8

B. Dey[a], N. Neri[a], and F. Palombo[ab]
INFN Sezione di Milano[a]; Dipartimento di Fisica, Università di Milano[b], I-20133 Milano, Italy

L. Cremaldi, R. Godang,[§] and D. J. Summers
University of Mississippi, University, Mississippi 38677, USA

P. Taras
Université de Montréal, Physique des Particules, Montréal, Québec, Canada H3C 3J7

G. De Nardo and C. Sciacca
INFN Sezione di Napoli and Dipartimento di Scienze Fisiche, Università di Napoli Federico II, I-80126 Napoli, Italy

G. Raven
NIKHEF, National Institute for Nuclear Physics and High Energy Physics, NL-1009 DB Amsterdam, The Netherlands

C. P. Jessop and J. M. LoSecco
University of Notre Dame, Notre Dame, Indiana 46556, USA

K. Honscheid and R. Kass
Ohio State University, Columbus, Ohio 43210, USA

A. Gaz[a], M. Margoni[ab], M. Posocco[a], M. Rotondo[a], G. Simi[ab], F. Simonetto[ab], and R. Stroili[ab]
INFN Sezione di Padova[a]; Dipartimento di Fisica, Università di Padova[b], I-35131 Padova, Italy

S. Akar, E. Ben-Haim, M. Bomben, G. R. Bonneaud, G. Calderini, J. Chauveau, G. Marchiori, and J. Ocariz
Laboratoire de Physique Nucléaire et de Hautes Energies, IN2P3/CNRS, Université Pierre et Marie Curie-Paris6, Université Denis Diderot-Paris7, F-75252 Paris, France

M. Biasini[ab], E. Manoni[a], and A. Rossi[a]
INFN Sezione di Perugia[a]; Dipartimento di Fisica, Università di Perugia[b], I-06123 Perugia, Italy

G. Batignani[ab], S. Bettarini[ab], M. Carpinelli[ab],¶ G. Casarosa[ab], M. Chrzaszcz[a], F. Forti[ab], M. A. Giorgi[ab], A. Lusiani[ac], B. Oberhof[ab], E. Paoloni[ab], M. Rama[a], G. Rizzo[ab], and J. J. Walsh[a]
INFN Sezione di Pisa[a]; Dipartimento di Fisica, Università di Pisa[b]; Scuola Normale Superiore di Pisa[c], I-56127 Pisa, Italy

A. J. S. Smith
Princeton University, Princeton, New Jersey 08544, USA

F. Anulli[a], R. Faccini[ab], F. Ferrarotto[a], F. Ferroni[ab], A. Pilloni[ab], and G. Piredda[a]
INFN Sezione di Roma[a]; Dipartimento di Fisica, Università di Roma La Sapienza[b], I-00185 Roma, Italy

C. Bünger, S. Dittrich, O. Grünberg, M. Heß, T. Leddig, C. Voß, and R. Waldi
Universität Rostock, D-18051 Rostock, Germany

T. Adye and F. F. Wilson
Rutherford Appleton Laboratory, Chilton, Didcot, Oxon, OX11 0QX, United Kingdom

S. Emery, G. Hamel de Monchenault, and G. Vasseur
CEA, Irfu, SPP, Centre de Saclay, F-91191 Gif-sur-Yvette, France

D. Aston, C. Cartaro, M. R. Convery, J. Dorfan, W. Dunwoodie, M. Ebert, R. C. Field, B. G. Fulsom, M. T. Graham, C. Hast, W. R. Innes, P. Kim, D. W. G. S. Leith, S. Luitz, V. Luth, D. B. MacFarlane, D. R. Muller, H. Neal, B. N. Ratcliff, A. Roodman, M. K. Sullivan, J. Va'vra, and W. J. Wisniewski

SLAC National Accelerator Laboratory, Stanford, California 94309 USA

M. V. Purohit and J. R. Wilson
University of South Carolina, Columbia, South Carolina 29208, USA

A. Randle-Conde and S. J. Sekula
Southern Methodist University, Dallas, Texas 75275, USA

M. Bellis, P. R. Burchat, and E. M. T. Puccio
Stanford University, Stanford, California 94305, USA

M. S. Alam and J. A. Ernst
State University of New York, Albany, New York 12222, USA

R. Gorodeisky, N. Guttman, D. R. Peimer, and A. Soffer
Tel Aviv University, School of Physics and Astronomy, Tel Aviv, 69978, Israel

S. M. Spanier
University of Tennessee, Knoxville, Tennessee 37996, USA

J. L. Ritchie and R. F. Schwitters
University of Texas at Austin, Austin, Texas 78712, USA

J. M. Izen and X. C. Lou
University of Texas at Dallas, Richardson, Texas 75083, USA

F. Bianchi[ab], F. De Mori[ab], A. Filippi[a], and D. Gamba[ab]
INFN Sezione di Torino[a]; Dipartimento di Fisica, Università di Torino[b], I-10125 Torino, Italy

L. Lanceri and L. Vitale
INFN Sezione di Trieste and Dipartimento di Fisica, Università di Trieste, I-34127 Trieste, Italy

F. Martinez-Vidal and A. Oyanguren
IFIC, Universitat de Valencia-CSIC, E-46071 Valencia, Spain

J. Albert, A. Beaulieu, F. U. Bernlochner, G. J. King, R. Kowalewski,
T. Lueck, I. M. Nugent, J. M. Roney, and N. Tasneem
University of Victoria, Victoria, British Columbia, Canada V8W 3P6

T. J. Gershon, P. F. Harrison, and T. E. Latham
Department of Physics, University of Warwick, Coventry CV4 7AL, United Kingdom

R. Prepost and S. L. Wu
University of Wisconsin, Madison, Wisconsin 53706, USA

We study the processes $\gamma\gamma\to K^0_S K^\pm\pi^\mp$ and $\gamma\gamma\to K^+K^-\pi^0$ using a data sample of 519 fb^{-1} recorded with the *BABAR* detector operating at the SLAC PEP-II asymmetric-energy e^+e^- collider at center-of-mass energies at and near the $\Upsilon(nS)$ $(n = 2, 3, 4)$ resonances. We observe η_c decays to both final states and perform Dalitz plot analyses using a model-independent partial wave analysis technique. This allows a model-independent measurement of the mass-dependence of the $I = 1/2$ $K\pi$ $\mathcal{S}$-wave amplitude and phase. A comparison between the present measurement and those from previous experiments indicates similar behaviour for the phase up to a mass of 1.5 GeV/c^2. In contrast, the amplitudes show very marked differences. The data require the presence of a new $a_0(1950)$ resonance with parameters $m = 1931 \pm 14 \pm 22$ MeV/c^2 and $\Gamma = 271 \pm 22 \pm 29$ MeV.

PACS numbers: 13.25.Gv, 14.40.Pq, 14.40.Df, 14.40.Be

*Also at: Thomas Jefferson National Accelerator Facility, Newport News, Virginia 23606, USA

I. INTRODUCTION

Scalar mesons are still a puzzle in light meson spectroscopy: they have complex structure, and there are too many states to be accommodated within the quark model without difficulty [1]. In particular, the structure of the $I = 1/2$ $K\pi$ $\mathcal{S}$-wave is a longstanding problem. In recent years many experiments have performed accurate studies of the decays of heavy-flavored hadrons producing a $K\pi$ system in the final state. These studies include searches for *CP* violation [2], and searches for, and observation of, new exotic resonances [3] and charmed mesons [4]. However, the still poorly known structure of the $I = 1/2$ $K\pi$ $\mathcal{S}$-wave is a source of large systematic uncertainties. The best source of information on the scalar structure of the $K\pi$ system comes from the LASS experiment, which studied the reaction $K^-p\to K^-\pi^+n$ [5]. Partial wave analysis of the $K\pi$ system reveals a large contribution from the $I = 1/2$ $K\pi$ $\mathcal{S}$-wave amplitude over the mass range studied. In the description of the $I = 1/2$ scalar amplitude up to a $K\pi$ mass of about 1.5 GeV/c^2 the $K_0^*(1430)$ resonant amplitude is added coherently to an effective-range description in such a way that the net amplitude actually decreases rapidly at the resonance mass. The $I = 1/2$ $\mathcal{S}$-wave amplitude representation is given explicitly in Ref. [6]. In the LASS analysis, in the region above 1.82 GeV/c^2, the $\mathcal{S}$-wave suffers from a two-fold ambiguity, but in both solutions it is understood in terms of the presence of a $K_0^*(1950)$ resonance. It should be noted that the extraction of the $I = 1/2$ $\mathcal{S}$-wave amplitude is complicated by the presence of an $I = 3/2$ contribution.

Further information on the $K\pi$ system has been extracted from Dalitz plot analysis of the decay $D^+\to K^-\pi^+\pi^+$ where, in order to fit the data, the presence of an additional resonance, the $\kappa(800)$, was claimed [7]. Using the same data, a Model Independent Partial Wave Analysis (MIPWA) of the $K\pi$ system was developed for the first time [8]. This method allows the amplitude and phase of the $K\pi$ $\mathcal{S}$-wave to be extracted as functions of mass (see also Refs. [9] and [10]). However in these analyses the phase space is limited to mass values less than 1.6 GeV/c^2 due to the kinematical limit imposed by the D^+ mass. A similar method has been used to extract the $\pi^+\pi^-$ $\mathcal{S}$-wave amplitude in a Dalitz plot analysis of $D_s^+\to\pi^+\pi^-\pi^+$ [11].

In the present analysis, we consider three-body η_c decays to $K\overline{K}\pi$ and obtain new information on the $K\pi$ $I = 1/2$ $\mathcal{S}$-wave amplitude extending up to a mass of 2.5 GeV/c^2. We emphasize that, due to isospin conservation in the η_c hadronic decay to $(K\pi)\overline{K}$, the $(K\pi)$ amplitude must have $I = 1/2$, and there is no $I = 3/2$ contribution. The *BABAR* experiment first performed a Dalitz plot analysis of $\eta_c\to K^+K^-\pi^0$ and $\eta_c\to K^+K^-\eta$ using an isobar model [12]. The analysis reported the first observation of $K_0^*(1430)\to K\eta$, and observed that η_c decays to three pseudoscalars are dominated by intermediate scalar mesons. A previous search for charmonium resonances decaying to $K_S^0K^\pm\pi^\mp$ in two-photon interactions is reported in Ref. [13]. We continue these studies of η_c decays and extract the $K\pi$ $\mathcal{S}$-wave amplitude by performing a MIPWA of both $\eta_c\to K_S^0K^\pm\pi^\mp$ and $\eta_c\to K^+K^-\pi^0$ final states.

We describe herein studies of the $K\overline{K}\pi$ system produced in two-photon interactions. Two-photon events in which at least one of the interacting photons is not quasi-real are strongly suppressed by the selection criteria described below. This implies that the allowed J^{PC} values of any produced resonances are $0^{\pm+}$, $2^{\pm+}$, 3^{++}, $4^{\pm+}$... [14]. Angular momentum conservation, parity conservation, and charge conjugation invariance imply that these quantum numbers also apply to the final state except that the $K\overline{K}\pi$ state cannot be in a $J^P = 0^+$ state.

This article is organized as follows. In Sec. II, a brief description of the *BABAR* detector is given. Section III is devoted to the event reconstruction and data selection of the $K_S^0K^\pm\pi^\mp$ system. In Sec. IV, we describe studies of efficiency and resolution, while in Sec. V we describe the MIPWA. In Secs. VI and VII we perform Dalitz plot analyses of $\eta_c\to K_S^0K^\pm\pi^\mp$ and $\eta_c\to K^+K^-\pi^0$ decays. Section VIII is devoted to discussion of the measured $K\pi$ $\mathcal{S}$-wave amplitude, and finally results are summarized in Sec. IX.

II. THE *BABAR* DETECTOR AND DATASET

The results presented here are based on data collected with the *BABAR* detector at the PEP-II asymmetric-energy e^+e^- collider located at SLAC, and correspond to an integrated luminosity of 519 fb^{-1} [15] recorded at center-of-mass energies at and near the $\Upsilon(nS)$ ($n = 2, 3, 4$) resonances. The *BABAR* detector is described in detail elsewhere [16]. Charged particles are detected, and their momenta are measured, by means of a five-layer, double-sided microstrip detector, and a 40-layer drift chamber, both operating in the 1.5 T magnetic field of a superconducting solenoid. Photons are measured and electrons are identified in a CsI(Tl) crystal electromagnetic calorimeter. Charged-particle identification is provided by the measurement of specific energy loss in the tracking devices, and by an internally reflecting, ring-imaging Cherenkov detector. Muons and K_L^0 mesons are detected in the instrumented flux return of the magnet. Monte Carlo (MC) simulated events [17], with reconstructed sample sizes more than 10 times larger than

[†]Now at: Università di Bologna and INFN Sezione di Bologna, I-47921 Rimini, Italy
[‡]Now at: University of Huddersfield, Huddersfield HD1 3DH, UK
[§]Now at: University of South Alabama, Mobile, Alabama 36688, USA
[¶]Also at: Università di Sassari, I-07100 Sassari, Italy

the corresponding data samples, are used to evaluate the signal efficiency and to determine background features. Two-photon events are simulated using the GamGam MC generator [18].

III. RECONSTRUCTION AND SELECTION OF $\eta_c \to K^0_S K^\pm \pi^\mp$ EVENTS

To study the reaction

$$\gamma\gamma \to K^0_S K^\pm \pi^\mp \tag{1}$$

we select events in which the e^+ and e^- beam particles are scattered at small angles, and hence are undetected in the final state. We consider only events for which the number of well-measured charged-particle tracks with transverse momentum greater than 0.1 GeV/c is exactly equal to four, and for which there are no more than five photon candidates with reconstructed energy in the electromagnetic calorimeter greater than 100 MeV. We obtain $K^0_S \to \pi^+\pi^-$ candidates by means of a vertex fit of pairs of oppositely charged tracks which requires a χ^2 fit probability greater than 0.001. Each K^0_S candidate is then combined with two oppositely charged tracks, and fitted to a common vertex, with the requirements that the fitted vertex be within the e^+e^- interaction region and have a χ^2 fit probability greater than 0.001. We select kaons and pions by applying high-efficiency particle identification criteria. We do not apply any particle identification requirements to the pions from the K^0_S decay. We accept only K^0_S candidates with decay lengths from the main vertex of the event greater than 0.2 cm, and require $\cos\theta_{K^0_S} > 0.98$, where $\theta_{K^0_S}$ is defined as the angle between the K^0_S momentum direction and the line joining the primary and the K^0_S vertex. A fit to the $\pi^+\pi^-$ mass spectrum using a linear function for the background and a Gaussian function with mean m and width σ gives $m = 497.24$ MeV/c^2 and $\sigma = 2.9$ MeV/c^2. We select the K^0_S signal region to be within $\pm 2\sigma$ of m and reconstruct the K^0_S 4-vector by adding the three-momenta of the pions and computing the energy using the K^0_S PDG mass value [19].

Background arises mainly from random combinations of particles from e^+e^- annihilation, from other two-photon processes, and from events with initial-state photon radiation (ISR). The ISR background is dominated by $J^{PC} = 1^{--}$ resonance production [20]. We discriminate against $K^0_S K^\pm \pi^\mp$ events produced via ISR by requiring $M^2_{\rm rec} \equiv (p_{e^+e^-} - p_{\rm rec})^2 > 10$ GeV$^2/c^4$, where $p_{e^+e^-}$ is the four-momentum of the initial state and $p_{\rm rec}$ is the four-momentum of the $K^0_S K^\pm \pi^\mp$ system.

The $K^0_S K^\pm \pi^\mp$ mass spectrum shows a prominent η_c signal. We define p_T as the magnitude of the vector sum of the transverse momenta, in the e^+e^- rest frame, of the final-state particles with respect to the beam axis. Since well-reconstructed two-photon events are expected to have low values of p_T, we optimize the selection as a function of this variable. We produce $K^0_S K^\pm \pi^\mp$ mass spectra with different p_T selections and fit the mass spectra to extract the number of η_c signal events (N_s) and the number of background events below the η_c signal (N_b). We then compute the purity, defined as $P = N_s/(N_s + N_b)$, and the significance $S = N_s/\sqrt{N_s + N_b}$. To obtain the best significance with the highest purity, we optimize the selection by requiring the maximum value of the product of purity and significance, $P \cdot S$, and find that this corresponds to the requirement $p_T < 0.08$ GeV/c.

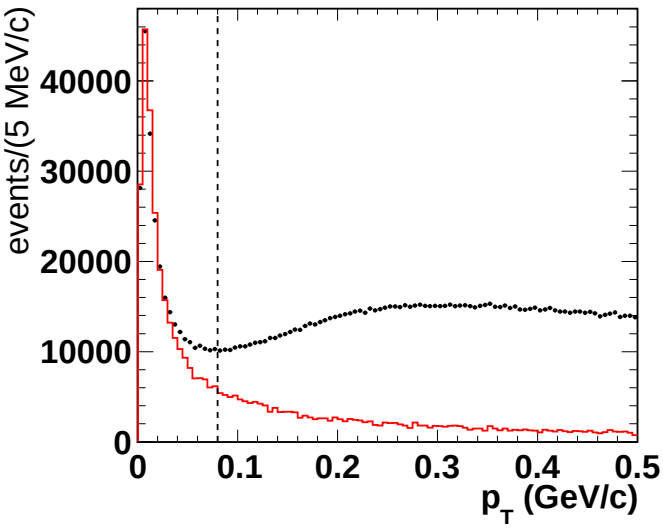

FIG. 1: Distributions of p_T for $\gamma\gamma \to K^0_S K^\pm \pi^\mp$. The data are shown as (black) points with error bars, and the signal MC simulation as a (red) histogram; the vertical dashed line indicates the selection applied to select two-photon events.

Figure 1 shows the measured p_T distribution in comparison to the corresponding p_T distribution obtained from simulation of the signal process. A peak at low p_T is observed indicating the presence of the two-photon process. The shape of the peak agrees well with that seen in the MC simulation. Figure 2 shows the $K^0_S K^\pm \pi^\mp$ mass spectrum in the η_c mass region. A clear η_c signal over a background of about 35% can be seen, together with a residual J/ψ signal. Information on the fitting procedure is given at the end of Sec. IV. We define the η_c signal region as the range 2.922-3.039 GeV/c^2 ($m(\eta_c) \pm 1.5\ \Gamma$), which contains 12849 events with a purity of $(64.3 \pm 0.4)\%$. Sideband regions are defined by the ranges 2.785-2.844 GeV/c^2 and 3.117-3.175 GeV/c^2 (within 3.5-5 Γ), respectively as indicated (shaded) in Fig. 2.

Details on data selection, event reconstruction, resolution, and efficiency measurement for the $\eta_c \to K^+K^-\pi^0$ decay can be found in Ref. [12]. The η_c signal region for this decay mode contains 6710 events with a purity of $(55.2 \pm 0.6)\%$.

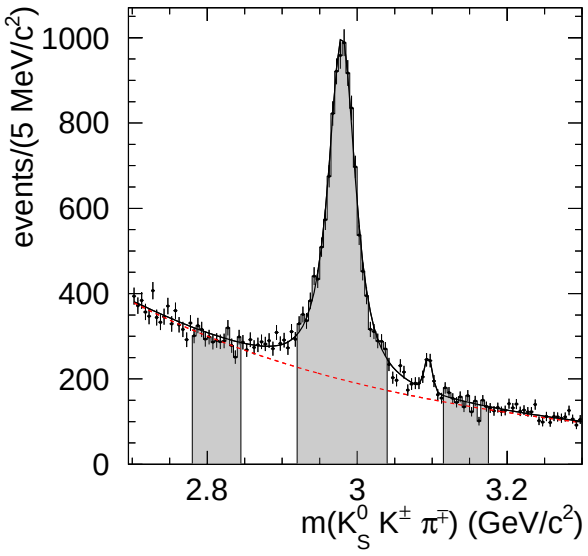

FIG. 2: The $K^0_S K^\pm \pi^\mp$ mass spectrum in the η_c mass region after requiring $p_T < 0.08$ GeV/c. The solid curve shows the total fitted function, and the dashed curve shows the fitted background contribution. The shaded areas show signal and sideband regions.

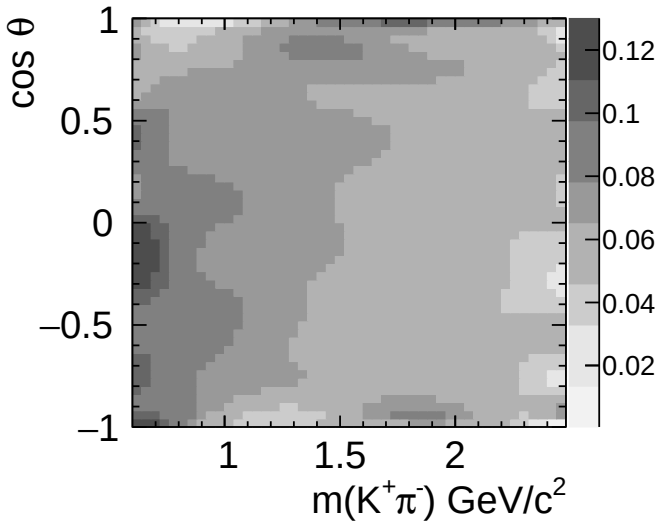

FIG. 3: Fitted detection efficiency in the $\cos\theta$ *vs.* $m(K^+\pi^-)$ plane. Each interval shows the average value of the fit for that region.

IV. EFFICIENCY AND RESOLUTION

To compute the efficiency, MC signal events are generated using a detailed detector simulation [17] in which the η_c decays uniformly in phase space. These simulated events are reconstructed and analyzed in the same manner as data. The efficiency is computed as the ratio of reconstructed to generated events. Due to the presence of long tails in the Breit-Wigner (BW) representation of the resonance, we apply selection criteria to restrict the generated events to the η_c mass region. We express the efficiency as a function of the invariant mass, $m(K^+\pi^-)$ [21], and $\cos\theta$, where θ is the angle, in the $K^+\pi^-$ rest frame, between the directions of the K^+ and the boost from the $K^0_S K^+\pi^-$ rest frame.

To smooth statistical fluctuations, this efficiency map is parametrized as follows. First we fit the efficiency as a function of $\cos\theta$ in separate intervals of $m(K^+\pi^-)$, using Legendre polynomials up to $L = 12$:

$$\epsilon(\cos\theta) = \sum_{L=0}^{12} a_L(m) Y^0_L(\cos\theta), \qquad (2)$$

where m denotes the $K^+\pi^-$ invariant mass. For each value of L, we fit the mass dependent coefficients $a_L(m)$ with a seventh-order polynomial in m. Figure 3 shows the resulting fitted efficiency map $\epsilon(m, \cos\theta)$. We obtain $\chi^2/N_{\rm cells} = 217/300$ for this fit, where $N_{\rm cells}$ is the number of cells in the efficiency map. We observe a significant decrease in efficiency in regions of $\cos\theta \sim \pm 1$ due to the impossibility of reconstructing $K^\pm$ mesons with laboratory momentum less than about 200 MeV/c, and $\pi^\pm$and $K^0_S(\to\pi^+\pi^-)$ mesons with laboratory momentum less than about 100 MeV/c (see Fig. 9 of Ref. [6]). These effects result from energy loss in the beampipe and inner-detector material.

The mass resolution, Δm, is measured as the difference between the generated and reconstructed $K^0_S K^\pm \pi^\mp$ invariant-mass values. The distribution has a root-mean-squared value of 10 MeV/c^2, and is parameterized by the sum of a Crystal Ball [22] and a Gaussian function. We perform a binned fit to the $K^0_S K^\pm \pi^\mp$ mass spectrum in data using the following model. The background is described by a second-order polynomial, and the η_c resonance is represented by a nonrelativistic BW function convolved with the resolution function. In addition, we allow for the presence of a residual J/ψ contribution modeled with a Gaussian function. Its parameter values are fixed to those obtained from a fit to the $K^0_S K^\pm \pi^\mp$ mass spectrum for the ISR data sample obtained by requiring $|M^2_{\rm rec}| < 1$ GeV$^2/c^4$. The fitted $K^0_S K^\pm \pi^\mp$ mass spectrum is shown in Fig. 2. We obtain the following η_c parameters:

$$\begin{aligned} m = 2980.8 \pm 0.4 \text{ MeV}/c^2,\ \Gamma = 33 \pm 1 \text{ MeV}, \\ N_{\eta_c} = 9808 \pm 164, \end{aligned} \qquad (3)$$

where uncertainties are statistical only. Our measured mass value is 2.8 MeV/c^2 lower than the world average [19]. This may be due to interference between the η_c amplitude and that describing the background in the

signal region [23].

V. MODEL INDEPENDENT PARTIAL WAVE ANALYSIS

We perform independent MIPWA of the $K^0_S K^\pm \pi^\mp$ and $K^+K^-\pi^0$ Dalitz plots in the η_c mass region using unbinned maximum likelihood fits. The likelihood function is written as

$$\mathcal{L} = \prod_{n=1}^{N} \left[f_{\rm sig}(m_n)\epsilon(x'_n, y'_n)\frac{\sum_{i,j} c_i c_j^* A_i(x_n, y_n)A_j^*(x_n, y_n)}{\sum_{i,j} c_i c_j^* I_{A_i A_j^*}} + (1 - f_{\rm sig}(m_n))\frac{\sum_i k_i B_i(x_n, y_n, m_n)}{\sum_i k_i I_{B_i}} \right] \quad (4)$$

where

- N is the number of events in the signal region;
- for the n-th event, m_n is the $K^0_S K^\pm\pi^\mp$ or the $K^+K^-\pi^0$ invariant mass;
- for the n-th event, $x_n = m^2(K^+\pi^-)$, $y_n = m^2(K^0_S\pi^-)$ for $K^0_S K^\pm\pi^\mp$; $x_n = m^2(K^+\pi^0)$, $y_n = m^2(K^-\pi^0)$ for $K^+K^-\pi^0$;
- $f_{\rm sig}$ is the mass-dependent fraction of signal obtained from the fit to the $K^0_S K^\pm\pi^\mp$ or $K^+K^-\pi^0$ mass spectrum;
- for the n-th event, $\epsilon(x'_n, y'_n)$ is the efficiency parametrized as a function of $x'_n = m(K^+\pi^-)$ for $K^0_S K^\pm\pi^\mp$ and $x'_n = m(K^+K^-)$ for $K^+K^-\pi^0$, and $y'_n = \cos\theta$ (see Sec. IV);
- for the n-th event, the $A_i(x_n, y_n)$ describe the complex signal-amplitude contributions;
- c_i is the complex amplitude for the i-th signal component; the c_i parameters are allowed to vary during the fit process;
- for the n-th event, the $B_i(x_n, y_n)$ describe the background probability-density functions assuming that interference between signal and background amplitudes can be ignored;
- k_i is the magnitude of the i-th background component; the k_i parameters are obtained by fitting the sideband regions;
- $I_{A_i A_j^*} = \int A_i(x,y)A_j^*(x,y)\epsilon(x',y')\ {\rm d}x{\rm d}y$ and $I_{B_i} = \int B_i(x,y){\rm d}x{\rm d}y$ are normalization integrals. Numerical integration is performed on phase space generated events with η_c signal and background generated according to the experimental distributions. In case of MIPWA or when resonances have free parameters, integrals are re-computed at each minimization step. Background integrals and fits dealing with amplitudes having fixed resonance parameters are computed only once.

Amplitudes are described along the lines described in Ref. [24]. For an η_c meson decaying into three pseudoscalar mesons via an intermediate resonance r of spin J (i.e. $\eta_c \to Cr$, $r \to AB$), each amplitude $A_i(x,y)$ is represented by the product of a complex Breit-Wigner (BW) function and a real angular distribution function represented by the spherical harmonic function $\sqrt{2\pi}Y^0_J(\cos\theta)$; θ is the angle between the direction of A, in the rest frame of r, and the direction of C in the same frame. This form of the angular dependence results from angular momentum conservation in the rest frame of the η_c, which leads to the production of r with helicity 0.

It follows that

$$A_i(x,y) = BW(M_{AB})\sqrt{2\pi}Y^0_J(\cos\theta). \quad (5)$$

The function $BW(M_{AB})$ is a relativistic BW function of the form

$$BW(M_{AB}) = \frac{F_{\eta_c} F}{M_r^2 - M_{AB}^2 - iM_r\Gamma_{\rm tot}(M_{AB})} \quad (6)$$

where M_r is the mass of the resonance r, and $\Gamma_{\rm tot}(M_{AB})$ is its mass-dependent total width. In general, this mass dependence cannot be specified, and a constant value should be used. However, for a resonance such as the $K^*_0(1430)$, which is approximately elastic, we can use the partial width Γ_{AB}, and specify the mass-dependence as:

$$\Gamma_{AB} = \Gamma_r \left(\frac{p_{AB}}{p_r}\right)^{2J+1} \left(\frac{M_r}{M_{AB}}\right) F^2 \quad (7)$$

where

$$p_{AB} = \frac{\sqrt{(M_{AB}^2 - M_A^2 - M_B^2)^2 - 4M_A^2 M_B^2}}{2M_{AB}}. \quad (8)$$

and p_r is the value of p_{AB} when $M_{AB} = M_r$.

The form factors F_{η_c} and F attempt to model the underlying quark structure of the parent particle and the intermediate resonances. We set F_{η_c} to a constant value, while for F we use Blatt-Weisskopf penetration factors [25] (Table I), that depend on a single parameter R representing the meson "radius", for which we assume $R = 1.5\ {\rm GeV}^{-1}$. The $a_0(980)$ resonance is parameterized as a coupled-channel Breit-Wigner function whose parameters are taken from Ref. [26].

To measure the $I = 1/2$ $K\pi$ $\mathcal{S}$-wave we make use of a MIPWA technique first described in Ref. [8]. The $K\pi$ $\mathcal{S}$-wave, being the largest contribution, is taken as the reference amplitude. We divide the $K\pi$ mass spectrum into 30 equally-spaced mass intervals 60 MeV wide, and for each interval we add to the fit two new free parameters, the amplitude and the phase of the $K\pi$ $\mathcal{S}$-wave in that interval. We fix the amplitude to 1.0 and its phase to $\pi/2$ at an arbitrary point in the mass spectrum, for

TABLE I: Summary of the Blatt-Weisskopf penetration form factors.

Spin	F
0	1
1	$\frac{\sqrt{1+(R_r p_r)^2}}{\sqrt{1+(R_r p_{AB})^2}}$
2	$\frac{\sqrt{9+3(R_r p_r)^2+(R_r p_r)^4}}{\sqrt{9+3(R_r p_{AB})^2+(R_r p_{AB})^4}}$

which we choose interval 14, corresponding to a mass of 1.45 GeV/c^2. The number of associated free parameters is therefore 58.

Due to isospin conservation in the hadronic η_c and K^* decays, the $(K\pi)\overline{K}$ amplitudes are combined with positive signs, and so therefore are symmetrized with respect to the two $K^*\overline{K}$ modes. In particular we write the $K\pi$ $\mathcal{S}$-wave amplitudes as

$$A_{\mathcal{S}\text{-wave}} = \frac{1}{\sqrt{2}}(a_j^{K^+\pi^-} e^{i\phi_j^{K^+\pi^-}} + a_j^{\overline{K}^0\pi^-} e^{i\phi_j^{\overline{K}^0\pi^-}}), \quad (9)$$

where $a^{K^+\pi^-}(m) = a^{\overline{K}^0\pi^-}(m)$ and $\phi^{K^+\pi^-}(m) = \phi^{\overline{K}^0\pi^-}(m)$, for $\eta_c \to \overline{K}^0 K^+\pi^-$ [21] and

$$A_{\mathcal{S}\text{-wave}} = \frac{1}{\sqrt{2}}(a_j^{K^+\pi^0} e^{i\phi_j^{K^+\pi^0}} + a_j^{K^-\pi^0} e^{i\phi_j^{K^-\pi^0}}), \quad (10)$$

where $a^{K^+\pi^0}(m) = a^{K^-\pi^0}(m)$ and $\phi^{K^+\pi^0}(m) = \phi^{K^-\pi^0}(m)$, for $\eta_c \to K^+K^-\pi^0$. For both decay modes the bachelor kaon is in an orbital $\mathcal{S}$-wave with respect to the relevant $K\pi$ system, and so does not affect these amplitudes. The second amplitude in Eq.(9) is reduced because the $\overline{K}^0$ is observed as a K_S^0, but the same reduction factor applies to the first amplitude through the bachelor $\overline{K}^0$, so that the equality of the three-body amplitudes is preserved.

Other resonance contributions are described as above. The $K_2^*(1430)\overline{K}$ contribution is symmetrized in the same way as the $\mathcal{S}$-wave amplitude.

We perform MC simulations to test the ability of the method to find the correct solution. We generate $\eta_c \to K_S^0 K^\pm\pi^\mp$ event samples which yield reconstructed samples having the same size as the data sample, according to arbitrary mixtures of resonances, and extract the $K\pi$ $\mathcal{S}$-wave using the MIPWA method. We find that the fit is able to extract correctly the mass dependence of the amplitude and phase.

We also test the possibility of multiple solutions by starting the fit from random values or constant parameter values very far from the solution found by the fit. We find only one solution in both final states and conclude that the fit converges to give the correct $\mathcal{S}$-wave behaviour for different starting values of the parameters.

The efficiency-corrected fractional contribution f_i due to resonant or non-resonant contribution i is defined as follows:

$$f_i = \frac{|c_i|^2 \int |A_i(x_n, y_n)|^2 \mathrm{d}x\mathrm{d}y}{\int |\sum_j c_j A_j(x,y)|^2 \mathrm{d}x\mathrm{d}y}. \quad (11)$$

The f_i do not necessarily sum to 100% because of interference effects. The uncertainty for each f_i is evaluated by propagating the full covariance matrix obtained from the fit.

We test the quality of the fit by examining a large sample of MC events at the generator level weighted by the likelihood fitting function and by the efficiency. These events are used to compare the fit result to the Dalitz plot and its projections with proper normalization. In these MC simulations we smooth the fitted $K\pi$ $\mathcal{S}$-wave amplitude and phase by means of a cubic spline. We make use of these weighted events to compute a 2-D χ^2 over the Dalitz plot. For this purpose, we divide the Dalitz plot into a grid of 25×25 cells and consider only those containing at least five events. We compute $\chi^2 = \sum_{i=1}^{N_{\text{cells}}} (N^i_{\text{obs}} - N^i_{\text{exp}})^2 / N^i_{\text{exp}}$, where N^i_{obs} and N^i_{exp} are event yields from data and simulation, respectively.

VI. DALITZ PLOT ANALYSIS OF $\eta_c \to K_S^0 K^\pm\pi^\mp$

Figure 4 shows the Dalitz plot for the candidates in the η_c signal region, and Fig. 5 shows the corresponding Dalitz plot projections. Since the width of the η_c meson is 32.3 ± 1.0 MeV, no mass constraint can be applied.

The Dalitz plot is dominated by the presence of horizontal and vertical uniform bands at the position of the $K_0^*(1430)$ resonance. We also observe further bands along the diagonal. Isospin conservation in η_c decay requires that the $(K\overline{K})$ system have I=1, so that these structures may indicate the presence of a_0 or a_2 resonances. Further narrow bands are observed at the position of the $K^*(892)$ resonance, mostly in the $K_S^0\pi^-$ projection; these components are consistent with originating from background, as will be shown.

The presence of background in the η_c signal region requires precise study of its structure. This can be achieved by means of the data in the η_c sideband regions, for which the Dalitz plots are shown in Fig. 6.

In both regions we observe almost uniformly populated resonant structures mostly in the $K_S^0\pi^-$ mass, especially in the regions corresponding to the $K^*(892)$‘¡ and $K_2^*(1430)$ resonances. The resonant structures in $K^+\pi^-$ mass are weaker. The three-body decay of a pseudoscalar meson into a spin-one or spin-two resonance yields a non-uniform distribution (see Eq. 5) in the relevant resonance band on the Dalitz plot. The presence of uniformly populated bands in the $K^*(892)$ and $K_2^*(1430)$ mass regions,

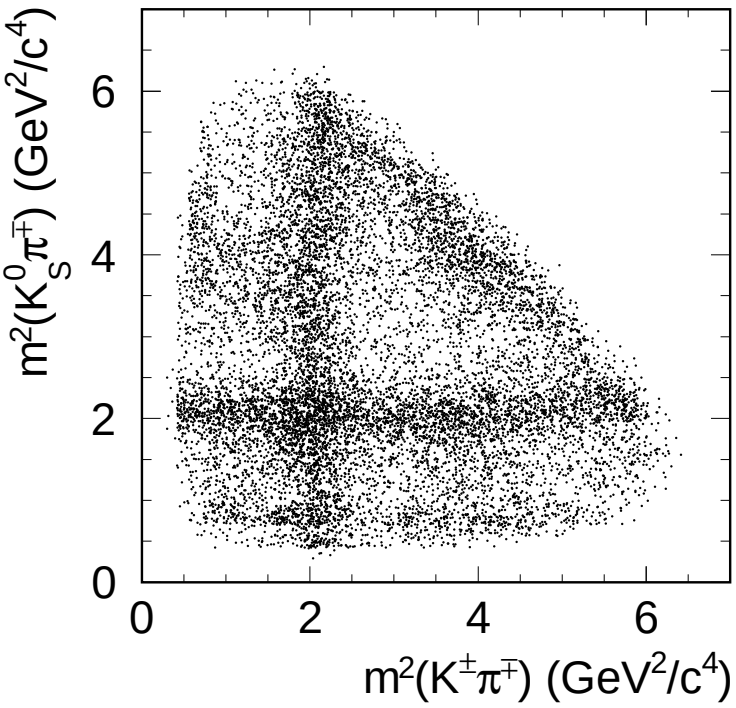

FIG. 4: Dalitz plot for $\eta_c \to K^0_S K^\pm \pi^\mp$ events in the signal region.

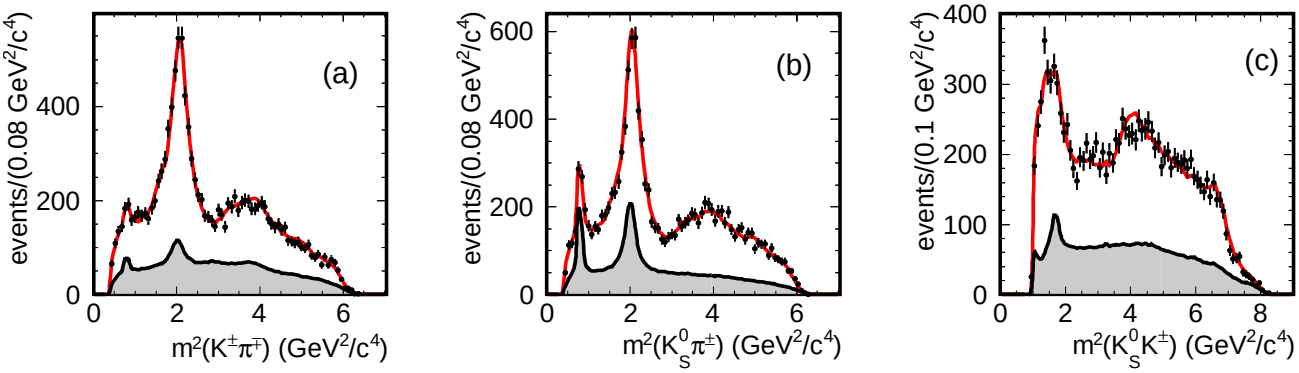

FIG. 5: The $\eta_c \to K^0_S K^\pm \pi^\mp$ Dalitz plot projections on (a) $m^2(K^\pm\pi^\mp)$, (b) $m^2(K^0_S\pi^\pm)$, and (c) $m^2(K^0_S K^\pm)$. The superimposed curves result from the MIPWA described in the text. The shaded regions show the background estimates obtained by interpolating the results of the Dalitz plot analyses of the sideband regions.

indicates that these structures are associated with background. Also, the asymmetry between the two K^* modes in background may be explained as being due to interference between the $I = 0$ and $I = 1$ isospin configurations for the $K^*(\to K\pi)\overline{K}$ final state produced in two-photon fusion.

We fit the η_c sidebands using an incoherent sum of amplitudes, which includes contributions from the $a_0(980)$, $a_0(1450)$, $a_2(1320)$, $K^*(892)$, $K^*_0(1430)$, $K^*_2(1430)$, $K^*(1680)$, and $K^*_0(1950)$ resonances. To better constrain the sum of the fractions to one, we make use of the channel likelihood method [27] and include resonances until no structure is left in the background and an accurate description of the Dalitz plots is obtained.

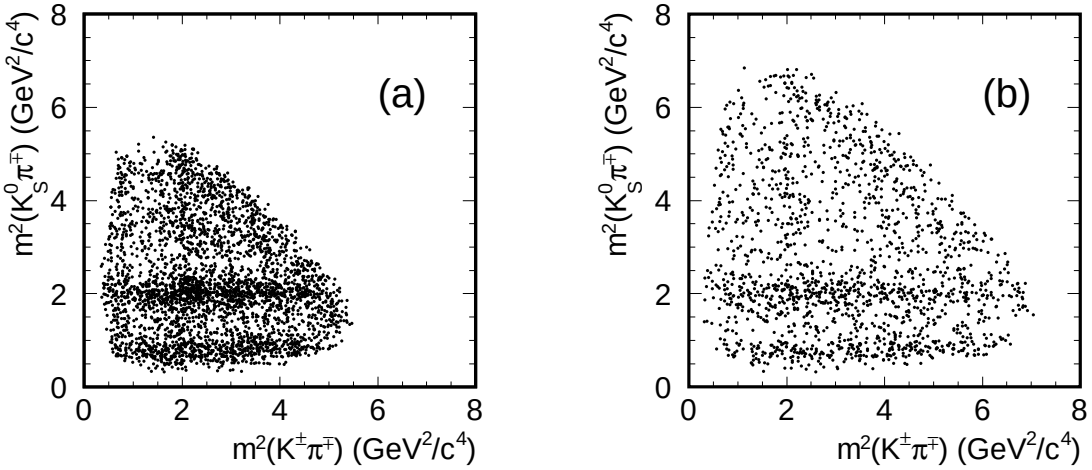

FIG. 6: Dalitz plots for the $\eta_c \to K^0_S K^\pm \pi^\mp$ sideband regions: (a) lower, (b) upper.

To estimate the background composition in the η_c signal region we perform a linear mass dependent interpolation of the fractions of the different contributions, obtained from the fits to the sidebands, and normalized using the results from the fit to the $K^0_S K^\pm \pi^\mp$ mass spectrum. The estimated background contributions are indicated by the shaded regions in Fig. 5.

A. MIPWA of $\eta_c \to K^0_S K^\pm \pi^\mp$

We perform the MIPWA including the resonances listed in Table II. In this table, and in the remainder of the paper, we use the notation $(K\pi)\overline{K}$ or $K^*\overline{K}$ to represent the corresponding symmetrized amplitude. After the solution is found we test for other contributions, including spin-one resonances, but these are found to be consistent with zero, and so are not included. This supports the observation that the observed $K^*(892)$ structures originate entirely from background. We find a dominance of the $K\pi$ $\mathcal{S}$-wave amplitude, with small contributions from $a_0\pi$ amplitudes and a significant $K^*_2(1430)\overline{K}$ contribution.

The table lists also a significant contribution from the $a_0(1950)\pi$ amplitude, where $a_0(1950)^+ \to K^0_S K^+$ is a new resonance. We also test the spin-2 hypothesis for this contribution by replacing the amplitude for $a_0 \to K^0_S K^+$ with an $a_2 \to K^0_S K^+$ amplitude with parameter values left free in the fit. In this case no physical solution is found inside the allowed ranges of the parameters, and the additional contribution is found consistent with zero. This new state has isospin one, and the spin-0 assignment is preferred over that of spin-2.

A fit without this state gives a poor description of the high mass $K^0_S K^+$ projection, as can be seen in Fig. 7(a). We obtain $-2\log\mathcal{L} = -4252.9$ and $\chi^2/N_{\rm cells} = 1.33$ for this fit. We then include in the MIPWA a new scalar resonance decaying to $K^0_S K^+$ with free parameters. We obtain $\Delta(\log\mathcal{L}) = 61$ and $\Delta\chi^2 = 38$ for an increase of four new parameters. We estimate the significance for the $a_0(1950)$ resonance using the fitted fraction divided by its statistical and systematic errors added in quadrature, and obtain 2.5σ. Since interference effects may also contribute to the significance, this procedure gives a conservative estimate. The systematic uncertainties associated with the $a_0(1950)$ state are described below. The fitted parameter values for this state are given in Table III. We note that we obtain $\chi^2/N_{\rm cells} = 1.17$ for this final fit, indicating good description of the data. The fit projections on the three squared masses from the MIPWA are shown in Fig. 5, and they indicate that the description of the data is quite good.

We compute the uncorrected Legendre polynomial moments $\langle Y^0_L \rangle$ in each $K^+\pi^-$, $K^0_S\pi^-$ and $K^0_S K^+$ mass interval by weighting each event by the relevant $Y^0_L(\cos\theta)$ function. These distributions are shown in Fig. 8 as functions of $K\pi$ mass after combining $K^+\pi^-$ and $K^0_S\pi^-$, and in Fig. 9 as functions of $K^0_S K^+$ mass. We also compute the expected Legendre polynomial moments from the weighted MC events and compare with the experimental distributions. We observe good agreement for all the distributions, which indicates that the fit is able to reproduce the local structures apparent in the Dalitz plot.

We compute the following systematic uncertainties on the $I = 1/2$ $K\pi$ $\mathcal{S}$-wave amplitude and phase. The different contributions are added in quadrature.

- Starting from the solution found by the fit, we generate MC simulated events which are fitted using a MIPWA. In this way we estimate the bias introduced by the fitting method.

TABLE II: Results from the $\eta_c \to K^0_S K^\pm \pi^\mp$ and $\eta_c \to K^+K^-\pi^0$ MIPWA. Phases are determined relative to the ($K\pi$ $\mathcal{S}$-wave) $\overline{K}$ amplitude which is fixed to $\pi/2$ at 1.45 GeV/c^2.

	$\eta_c \to K^0_S K^\pm \pi^\mp$		$\eta_c \to K^+K^-\pi^0$	
Amplitude	Fraction (%)	Phase (rad)	Fraction (%)	Phase (rad)
($K\pi$ $\mathcal{S}$-wave) $\overline{K}$	107.3 ± 2.6 ± 17.9	fixed	125.5 ± 2.4 ± 4.2	fixed
$a_0(980)\pi$	0.8 ± 0.5 ± 0.8	1.08 ± 0.18 ± 0.18	0.0 ± 0.1 ± 1.7	-
$a_0(1450)\pi$	0.7 ± 0.2 ± 1.4	2.63 ± 0.13 ± 0.17	1.2 ± 0.4 ± 0.7	2.90 ± 0.12 ± 0.25
$a_0(1950)\pi$	3.1 ± 0.4 ± 1.2	−1.04 ± 0.08 ± 0.77	4.4 ± 0.8 ± 0.8	−1.45 ± 0.08 ± 0.27
$a_2(1320)\pi$	0.2 ± 0.1 ± 0.1	1.85 ± 0.20 ± 0.20	0.6 ± 0.2 ± 0.3	1.75 ± 0.23 ± 0.42
$K_2^*(1430)\overline{K}$	4.7 ± 0.9 ± 1.4	4.92 ± 0.05 ± 0.10	3.0 ± 0.8 ± 4.4	5.07 ± 0.09 ± 0.30
Total	116.8 ± 2.8 ± 18.1		134.8 ± 2.7 ± 6.4	
$-2\log\mathcal{L}$	−4314.2		−2339	
$\chi^2/N_{\rm cells}$	301/254=1.17		283.2/233=1.22	

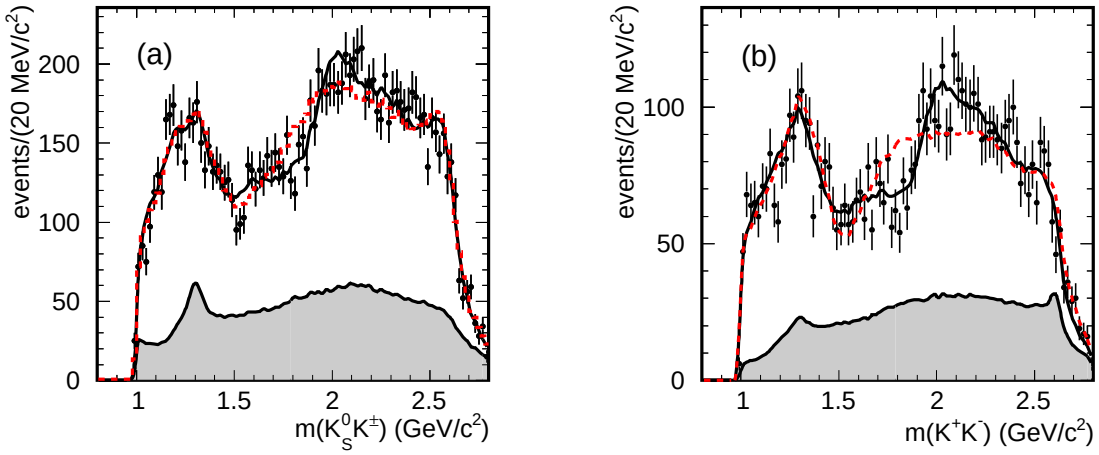

FIG. 7: The mass projections (a) $K^0_S K^\pm$ from $\eta_c \to K^0_S K^\pm \pi^\mp$ and (b) K^+K^- from $\eta_c \to K^+K^-\pi^0$. The histograms show the MIPWA fit projections with (solid, black) and without (dashed, red) the presence of the $a_0(1950)^+ \to K^0_S K^\pm$ resonance. The shaded regions show the background estimates obtained by interpolating the results of the Dalitz plot analyses of the sideband regions.

TABLE III: Fitted $a_0(1950)$ parameter values for the two η_c decay modes.

Final state	Mass (MeV/c^2)	Width (MeV)
$\eta_c \to K^0_S K^\pm \pi^\mp$	1949 ± 32 ± 76	265 ± 36 ± 110
$\eta_c \to K^+K^-\pi^0$	1927 ± 15 ± 23	274 ± 28 ± 30
Weighted mean	1931 ± 14 ± 22	271 ± 22 ± 29

- The fit is performed by interpolating the $K\pi$ $\mathcal{S}$-wave amplitude and phase using a cubic spline.
- We remove low-significance contributions, such as those from the $a_0(980)$ and $a_2(1320)$ resonances.
- We vary the signal purity up and down according to its statistical uncertainty.
- The effect of the efficiency variation as a function of $K\overline{K}\pi$ mass is evaluated by computing separate efficiencies in the regions below and above the η_c mass.

These additional fits also allow the computation of systematic uncertainties on the amplitude fraction and phase values, as well as on the parameter values for the $a_0(1950)$ resonance; these are summarized in Table IV. In the evaluation of overall systematic uncertainties, all effects are assumed to be uncorrelated, and are added in quadrature.

The measured amplitude and phase values of the $I = 1/2$ $K\pi$ $\mathcal{S}$-wave as functions of mass obtained from the MIPWA of $\eta_c \to K^0_S K^\pm \pi^\mp$ are shown in Table V. Interval

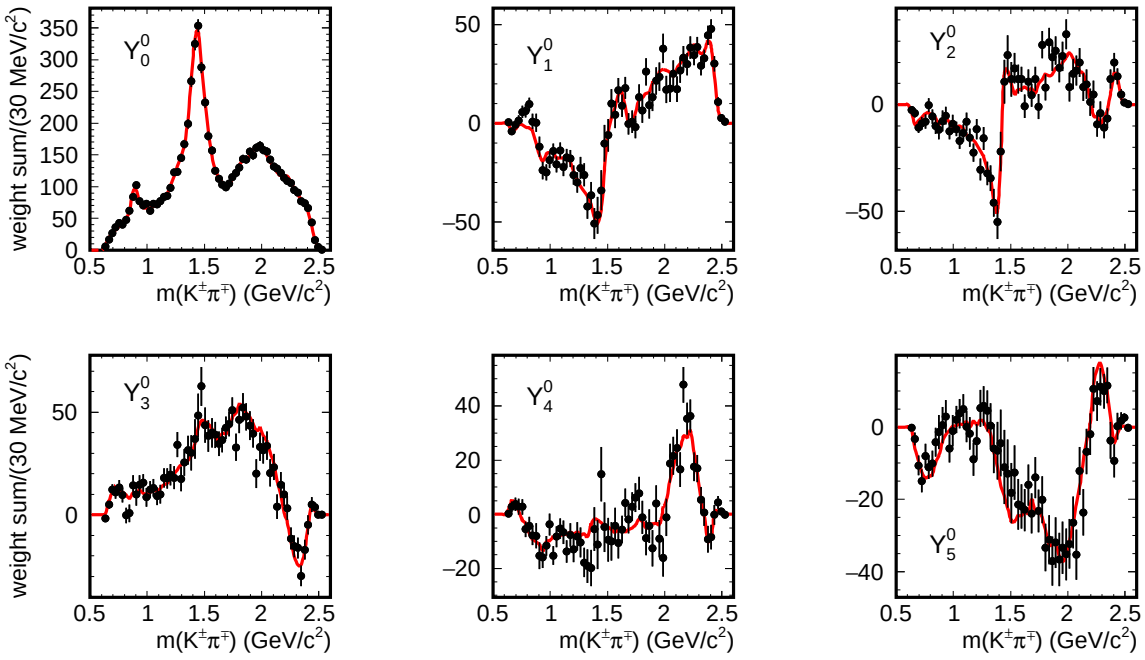

FIG. 8: Legendre polynomial moments for $\eta_c \to K^0_S K^\pm \pi^\mp$ as functions of $K\pi$ mass, and combined for $K^\pm\pi^\mp$ and $K^0_S\pi^\mp$; the superimposed curves result from the Dalitz plot fit described in the text.

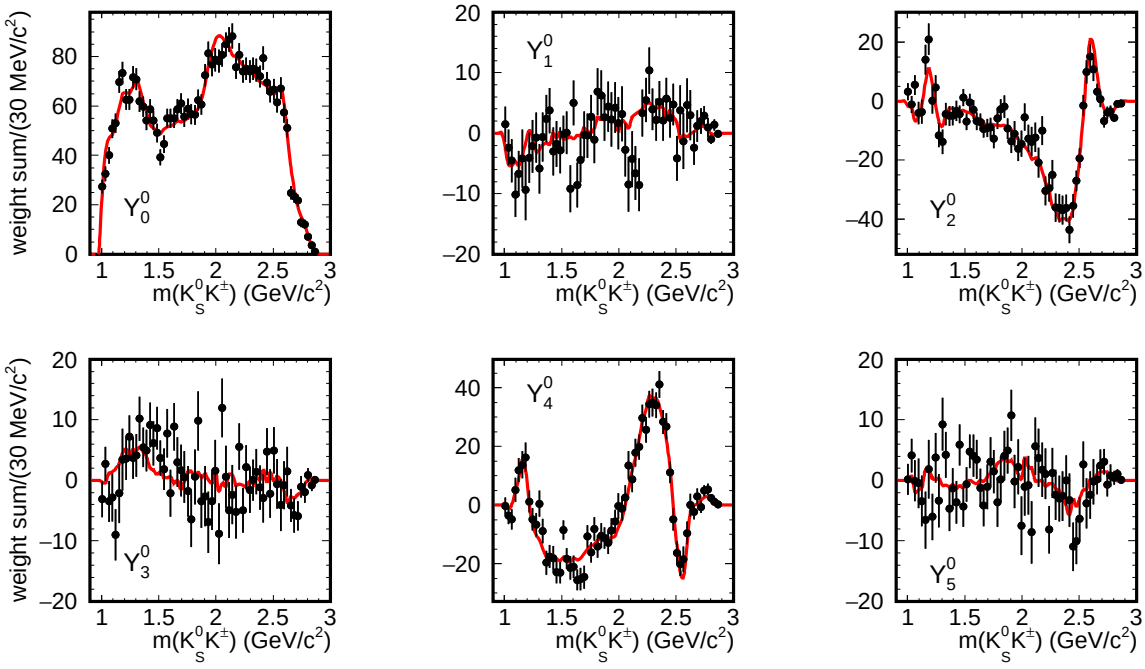

FIG. 9: Legendre polynomial moments for $\eta_c \to K^0_S K^\pm \pi^\mp$ as a function of $K^0_S K^\pm$ mass, the superimposed curves result from the Dalitz plot fit described in the text.

14 of the $K\pi$ mass contains the fixed amplitude and phase values.

B. Dalitz plot analysis of $\eta_c \to K^0_S K^\pm \pi^\mp$ using an isobar model

We perform a Dalitz plot analysis of $\eta_c \to K^0_S K^\pm \pi^\mp$ using a standard isobar model, where all resonances are modeled as BW functions multiplied by the corresponding angular functions. In this case the $K\pi$ $\mathcal{S}$-wave is represented by a superposition of interfering $K^*_0(1430)$, $K^*_0(1950)$, non-resonant (NR), and possibly $\kappa(800)$ contributions. The NR contribution is parametrized as an amplitude that is constant in magnitude and phase over the Dalitz plot. In this fit the $K^*_0(1430)$ parameters are taken from Ref. [12], while all other parameters are fixed to PDG values. We also add the $a_0(1950)$ resonance with parameters obtained from the MIPWA analysis.

For the description of the η_c signal, amplitudes are added one by one to ascertain the associated increase of the likelihood value and decrease of the 2-D χ^2. Table VI summarizes the fit results for the amplitude fractions and phases. The high value of $\chi^2/N_{\rm cells} = 1.82$ (to be compared with $\chi^2/N_{\rm cells} = 1.17$) indicates a poorer description of the data than that obtained with the MIPWA method. Including the $\kappa(800)$ resonance does not improve the fit quality. If included, it gives a fit fraction of $(0.8 \pm 0.5)\%$.

The Dalitz plot analysis shows a dominance of scalar meson amplitudes, with small contributions from spin-two resonances. The $K^*(892)$ contribution is consistent with originating entirely from background. Other spin-1 K^* resonances have been included in the fit, but their contributions have been found to be consistent with zero. We note the presence of a sizeable non-resonant contribution. However, in this case the sum of the fractions is significantly lower than 100%, indicating important interference effects. Fitting the data without the NR contribution gives a much poorer description, with $-2\log\mathcal{L} = -4115$ and $\chi^2/N_{\rm cells} = 2.32$.

We conclude that the $\eta_c \to K^0_S K^\pm \pi^\mp$ Dalitz plot is not well-described by an isobar model in which the $K\pi$ $\mathcal{S}$-wave is modeled as a superposition of Breit-Wigner functions. A more complex approach is needed, and the MIPWA is able to describe this amplitude without the need for a specific model.

VII. DALITZ PLOT ANALYSIS OF $\eta_c \to K^+K^-\pi^0$

The $\eta_c \to K^+K^-\pi^0$ Dalitz plot [12] is very similar to that for $\eta_c \to K^0_S K^\pm \pi^\mp$ decays. It is dominated by uniformly populated bands at the $K^*_0(1430)$ resonance position in $K^+\pi^0$ and $K^-\pi^0$ mass squared. It also shows a broad diagonal structure indicating the presence of a_0 or a_2 resonance contributions. The Dalitz plot projections are shown in Fig. 10.

The $\eta_c \to K^+K^-\pi^0$ Dalitz plot analysis using the isobar model has been performed already in Ref. [12] . It was found that the model does not give a perfect description of the data. In this section we obtain a new measurement of the $K\pi$ $\mathcal{S}$-wave by making use of the MIPWA method. In this way we also perform a cross-check of the results obtained from the $\eta_c \to K^0_S K^\pm \pi^\mp$ analysis, since analyses of the two η_c decay modes should give consistent results, given the absence of I=3/2 $K\pi$ amplitude contributions.

A. MIPWA of $\eta_c \to K^+K^-\pi^0$

We perform a MIPWA of $\eta_c \to K^+K^-\pi^0$ decays using the same model and the same mass grid as for $\eta_c \to K^0_S K^\pm \pi^\mp$. As for the previous case we obtain a better description of the data if we include an additional $a_0(1950)$ resonance, whose parameter values are listed in Table III. We observe good agreement between the parameter values obtained from the two η_c decay modes. The table also lists parameter values obtained as the weighted mean of the two measurements. Table II gives the fitted fractions from the MIPWA fit.

We obtain a good description of the data, as evidenced by the value $\chi^2/N_{\rm cells} = 1.22$, and observe the $a_0(1950)$ state with a significance of 4.2σ. The fit projections on the $K^+\pi^0$, $K^-\pi^0$, and K^+K^- squared mass distributions are shown in Fig. 10. As previously, there is a dominance of the ($K\pi$ $\mathcal{S}$-wave) $\overline{K}$ amplitude, with a significant $K^*_2(1430)\overline{K}$ amplitude, and small contributions from $a_0\pi$ amplitudes. We observe good agreement between fractions and relative phases of the amplitudes between the $\eta_c \to K^0_S K^\pm \pi^\mp$ and $\eta_c \to K^+K^-\pi^0$ decay modes. Systematic uncertainties are evaluated as discussed in Sec. VI.A.

We compute the uncorrected Legendre polynomial moments $\langle Y^0_L \rangle$ in each $K^+\pi^0$, $K^-\pi^0$ and K^+K^- mass interval by weighting each event by the relevant $Y^0_L(\cos\theta)$ function. These distributions are shown in Fig. 11 as functions of $K\pi$ mass, combined for $K^+\pi^0$ and $K^-\pi^0$, and in Fig. 12 as functions of K^+K^- mass. We also compute the expected Legendre polynomial moments from the weighted MC events and compare with the experimental distributions. We observe good agreement for all the distributions, which indicates that also in this case the fit is able to reproduce the local structures apparent in the Dalitz plot.

VIII. THE $I = 1/2$ $K\pi$ $\mathcal{S}$-WAVE AMPLITUDE AND PHASE

Figure 13 displays the measured $I = 1/2$ $K\pi$ $\mathcal{S}$-wave amplitude and phase from both $\eta_c \to K^0_S K^\pm \pi^\mp$ and $\eta_c \to K^+K^-\pi^0$. We observe good agreement between the amplitude and phase values obtained from the two measurements.

TABLE IV: Systematic uncertainties on the $a_0(1950)$ parameter values from the two η_c decay modes.

	$\eta_c \to K^0_S K^\pm \pi^\mp$			$\eta_c \to K^+ K^- \pi^0$		
Effect	Mass (MeV/c^2)	Width (MeV)	Fraction (%)	Mass (MeV/c^2)	Width (MeV)	Fraction (%)
Fit bias	11	22	0.5	1	10	0.5
Cubic spline	24	79	0.6	14	9	0.2
Marginal components	70	72	0.0	2	8	0.3
η_c purity	3	16	1.0	18	26	0.4
Efficiency	11	8	0.2	1	15	0.2
Total	76	110	1.3	23	30	0.8

TABLE V: Measured amplitude and phase values for the $I = 1/2$ $K\pi$ $\mathcal{S}$-wave as functions of mass obtained from the MIPWA of $\eta_c \to K^0_S K^\pm \pi^\mp$ and $\eta_c \to K^+ K^- \pi^0$. The first error is statistical, the second systematic. The amplitudes and phases in the mass interval 14 are fixed to constant values.

		$\eta_c \to K^0_S K^\pm \pi^\mp$		$\eta_c \to K^+ K^- \pi^0$	
N	$K\pi$ mass	Amplitude	Phase (rad)	Amplitude	Phase (rad)
1	0.67	$0.119 \pm 0.100 \pm 0.215$	$0.259 \pm 0.577 \pm 1.290$	$0.154 \pm 0.350 \pm 0.337$	$3.786 \pm 1.199 \pm 0.857$
2	0.73	$0.103 \pm 0.043 \pm 0.113$	$-0.969 \pm 0.757 \pm 1.600$	$0.198 \pm 0.124 \pm 0.216$	$3.944 \pm 0.321 \pm 0.448$
3	0.79	$0.158 \pm 0.086 \pm 0.180$	$0.363 \pm 0.381 \pm 1.500$	$0.161 \pm 0.116 \pm 0.098$	$1.634 \pm 0.584 \pm 0.448$
4	0.85	$0.232 \pm 0.128 \pm 0.214$	$0.448 \pm 0.266 \pm 1.500$	$0.125 \pm 0.118 \pm 0.031$	$3.094 \pm 0.725 \pm 0.448$
5	0.91	$0.468 \pm 0.075 \pm 0.194$	$0.091 \pm 0.191 \pm 0.237$	$0.307 \pm 0.213 \pm 0.162$	$0.735 \pm 0.326 \pm 0.255$
6	0.97	$0.371 \pm 0.083 \pm 0.129$	$0.276 \pm 0.156 \pm 0.190$	$0.528 \pm 0.121 \pm 0.055$	$-0.083 \pm 0.178 \pm 0.303$
7	1.03	$0.329 \pm 0.071 \pm 0.102$	$0.345 \pm 0.164 \pm 0.273$	$0.215 \pm 0.191 \pm 0.053$	$0.541 \pm 0.320 \pm 0.638$
8	1.09	$0.343 \pm 0.062 \pm 0.062$	$0.449 \pm 0.196 \pm 0.213$	$0.390 \pm 0.146 \pm 0.046$	$0.254 \pm 0.167 \pm 0.144$
9	1.15	$0.330 \pm 0.070 \pm 0.081$	$0.687 \pm 0.167 \pm 0.221$	$0.490 \pm 0.135 \pm 0.089$	$0.618 \pm 0.155 \pm 0.099$
10	1.21	$0.450 \pm 0.059 \pm 0.042$	$0.696 \pm 0.156 \pm 0.226$	$0.422 \pm 0.092 \pm 0.102$	$0.723 \pm 0.242 \pm 0.267$
11	1.27	$0.578 \pm 0.048 \pm 0.112$	$0.785 \pm 0.208 \pm 0.358$	$0.581 \pm 0.113 \pm 0.084$	$0.605 \pm 0.186 \pm 0.166$
12	1.33	$0.627 \pm 0.047 \pm 0.053$	$0.986 \pm 0.153 \pm 0.166$	$0.643 \pm 0.106 \pm 0.039$	$1.330 \pm 0.264 \pm 0.130$
13	1.39	$0.826 \pm 0.047 \pm 0.105$	$1.334 \pm 0.155 \pm 0.288$	$0.920 \pm 0.153 \pm 0.056$	$1.528 \pm 0.161 \pm 0.160$
14	1.45	1.000	1.570	1.000	1.570
15	1.51	$0.736 \pm 0.031 \pm 0.059$	$1.918 \pm 0.153 \pm 0.132$	$0.750 \pm 0.118 \pm 0.076$	$1.844 \pm 0.149 \pm 0.048$
16	1.57	$0.451 \pm 0.025 \pm 0.053$	$2.098 \pm 0.202 \pm 0.277$	$0.585 \pm 0.099 \pm 0.047$	$2.128 \pm 0.182 \pm 0.110$
17	1.63	$0.289 \pm 0.029 \pm 0.065$	$2.539 \pm 0.292 \pm 0.180$	$0.366 \pm 0.079 \pm 0.052$	$2.389 \pm 0.230 \pm 0.213$
18	1.69	$0.159 \pm 0.036 \pm 0.089$	$1.566 \pm 0.308 \pm 0.619$	$0.312 \pm 0.074 \pm 0.043$	$1.962 \pm 0.195 \pm 0.150$
19	1.75	$0.240 \pm 0.034 \pm 0.067$	$1.962 \pm 0.331 \pm 0.655$	$0.427 \pm 0.093 \pm 0.063$	$1.939 \pm 0.150 \pm 0.182$
20	1.81	$0.381 \pm 0.031 \pm 0.059$	$2.170 \pm 0.297 \pm 0.251$	$0.511 \pm 0.094 \pm 0.063$	$2.426 \pm 0.156 \pm 0.277$
21	1.87	$0.457 \pm 0.035 \pm 0.085$	$2.258 \pm 0.251 \pm 0.284$	$0.588 \pm 0.098 \pm 0.080$	$2.242 \pm 0.084 \pm 0.210$
22	1.93	$0.565 \pm 0.042 \pm 0.067$	$2.386 \pm 0.255 \pm 0.207$	$0.729 \pm 0.114 \pm 0.095$	$2.427 \pm 0.098 \pm 0.254$
23	1.99	$0.640 \pm 0.044 \pm 0.055$	$2.361 \pm 0.228 \pm 0.092$	$0.777 \pm 0.119 \pm 0.075$	$2.306 \pm 0.102 \pm 0.325$
24	2.05	$0.593 \pm 0.046 \pm 0.065$	$2.329 \pm 0.235 \pm 0.268$	$0.775 \pm 0.134 \pm 0.075$	$2.347 \pm 0.107 \pm 0.299$
25	2.11	$0.614 \pm 0.057 \pm 0.083$	$2.421 \pm 0.230 \pm 0.169$	$0.830 \pm 0.134 \pm 0.078$	$2.374 \pm 0.105 \pm 0.199$
26	2.17	$0.677 \pm 0.067 \pm 0.117$	$2.563 \pm 0.218 \pm 0.137$	$0.825 \pm 0.140 \pm 0.070$	$2.401 \pm 0.127 \pm 0.189$
27	2.23	$0.788 \pm 0.085 \pm 0.104$	$2.539 \pm 0.228 \pm 0.241$	$0.860 \pm 0.158 \pm 0.123$	$2.296 \pm 0.131 \pm 0.297$
28	2.29	$0.753 \pm 0.097 \pm 0.125$	$2.550 \pm 0.234 \pm 0.168$	$0.891 \pm 0.167 \pm 0.133$	$2.320 \pm 0.131 \pm 0.273$
29	2.35	$0.646 \pm 0.096 \pm 0.118$	$2.315 \pm 0.241 \pm 0.321$	$0.994 \pm 0.202 \pm 0.076$	$2.297 \pm 0.153 \pm 0.197$
30	2.41	$0.789 \pm 0.184 \pm 0.187$	$2.364 \pm 0.336 \pm 0.199$	$0.892 \pm 0.322 \pm 0.098$	$2.143 \pm 0.292 \pm 0.393$

The main features of the amplitude (Fig. 13(a)) can be explained by the presence of a clear peak related to the $K^*_0(1430)$ resonance which shows a rapid drop around 1.7 GeV/c^2, where a broad structure is present which can be related to the $K^*_0(1950)$ resonance. There is some indication of feedthrough from the $K^*(892)$ background. The phase motion (Fig. 13(b)) shows the expected behavior for the resonance phase, which varies by about π in the $K^*_0(1430)$ resonance region. The phase shows a drop around 1.7 GeV/c^2 related to interference with the $K^*_0(1950)$ resonance.

We compare the present measurement of the $K\pi$ $\mathcal{S}$-wave amplitude from $\eta_c \to K^0_S K^\pm \pi^\mp$ with measurements from LASS [5] in Fig. 14(a)(c) and E791 [8] in Fig. 14(b)(d). We plot only the first part of the LASS measurement since it suffers from a two-fold ambiguity

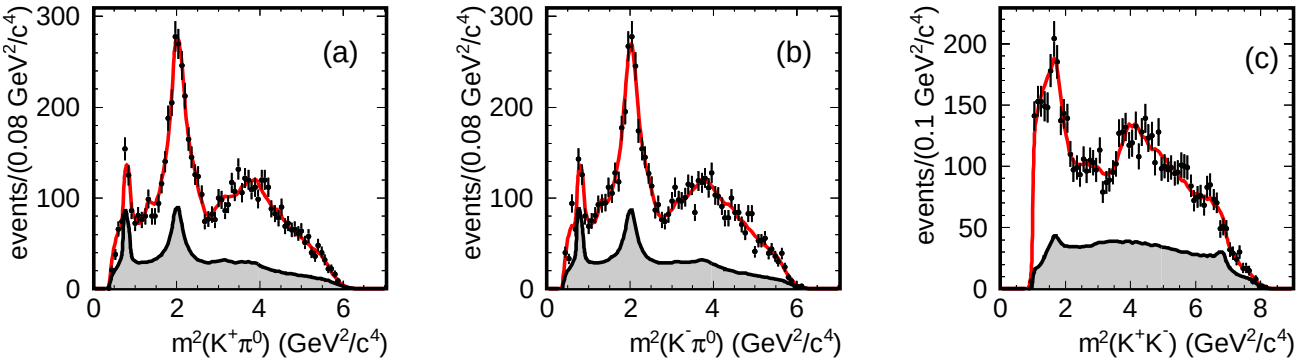

FIG. 10: The $\eta_c \to K^+K^-\pi^0$ Dalitz plot projections, (a) $m^2(K^+\pi^0)$, (b) $m^2(K^-\pi^0)$, and (c) $m^2(K^+K^-)$. The superimposed curves result from the MIPWA described in the text. The shaded regions show the background estimates obtained by interpolating the results of the Dalitz plot analyses of the sideband regions.

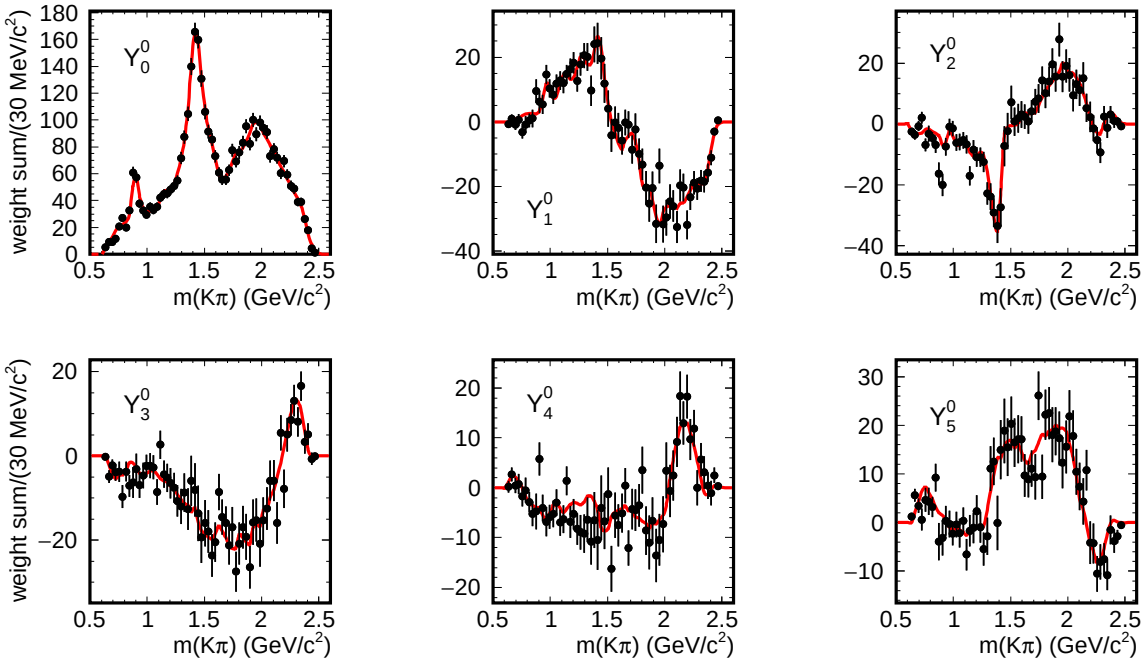

FIG. 11: Legendre polynomial moments for $\eta_c \to K^+K^-\pi^0$ as functions of $K\pi$ mass, combined for $K^+\pi^0$ and $K^-\pi^0$. The superimposed curves result from the Dalitz plot fit described in the text.

above the mass of 1.82 GeV/c^2. The Dalitz plot fits extract invariant amplitudes. Consequently, in Fig. 14(a), the LASS $I = 1/2$ $K\pi$ scattering amplitude values have been multiplied by the factor $m(K\pi)/q$ to convert to invariant amplitude, and normalized so as to equal the scattering amplitude at 1.5 GeV/c^2 in order to facilitate comparison to the η_c results. Here q is the momentum of either meson in the $K\pi$ rest frame. For better comparison, the LASS absolute phase measurements have been displaced by -0.6 rad before plotting them in Fig. 14(c). In Fig. 14(b) the E791 amplitude has been obtained by multiplying the amplitude c in Table III of Ref. [8] by the Form Factor F_D^0, for which the mass-dependence is motivated by theoretical speculation. This yields amplitude values corresponding to the E791 Form Factor having value 1, as for the η_c analyses. In Fig. 14(d), the E791 phase measurements have been displaced by $+0.9$ rad, again in order to facilitate comparison to the η_c measurements.

While we observe similar phase behavior among the

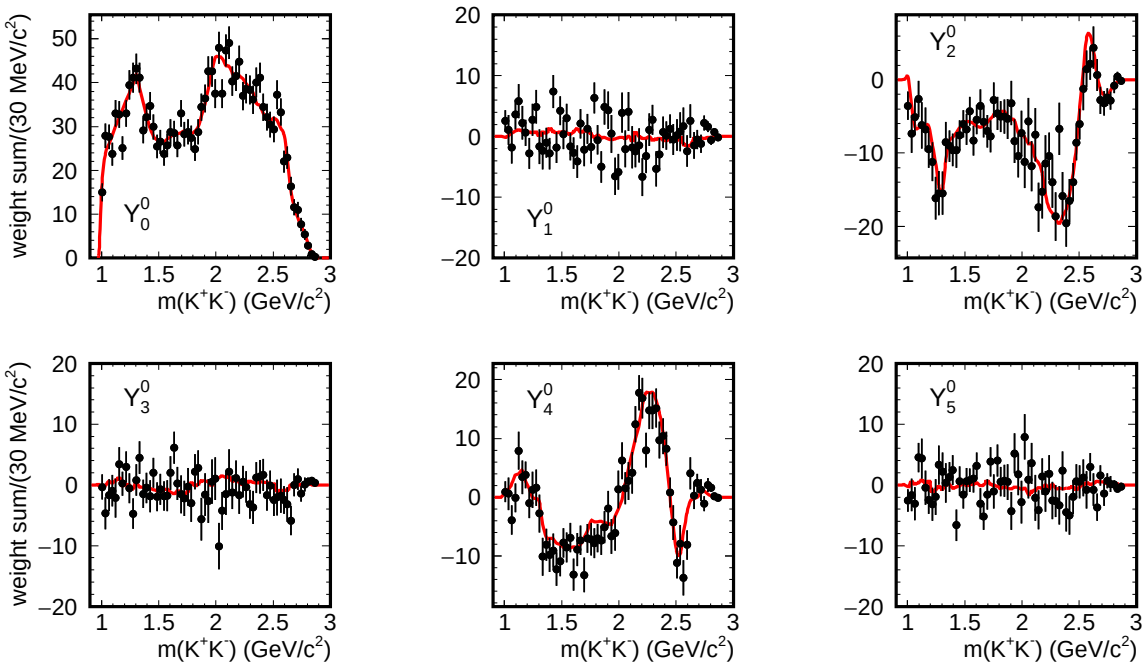

FIG. 12: Legendre polynomial moments for $\eta_c \to K^+K^-\pi^0$ as a function of K^+K^- mass. The superimposed curves result from the Dalitz plot fit described in the text.

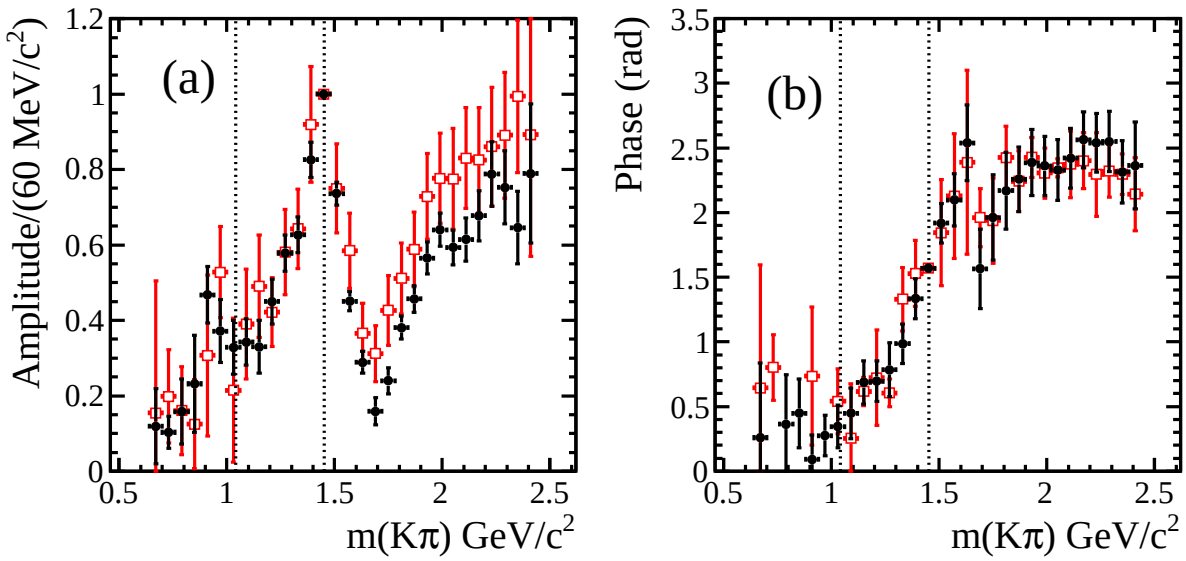

FIG. 13: The $I = 1/2$ $K\pi$ $\mathcal{S}$-wave amplitude (a) and phase (b) from $\eta_c \to K^0_S K^\pm \pi^\mp$ (solid (black) points) and $\eta_c \to K^+K^-\pi^0$ (open (red) points); only statistical uncertainties are shown. The dotted lines indicate the $K\eta$ and $K\eta'$ thresholds.

three measurements up to about 1.5 GeV/c^2, we observe striking differences in the mass dependence of the amplitudes.

IX. SUMMARY

We perform Dalitz plot analyses, using an isobar model and a MIPWA method, of data on the decays $\eta_c \to K^0_S K^\pm \pi^\mp$ and $\eta_c \to K^+K^-\pi^0$, where the η_c mesons are produced in two-photon interactions in the *BABAR*

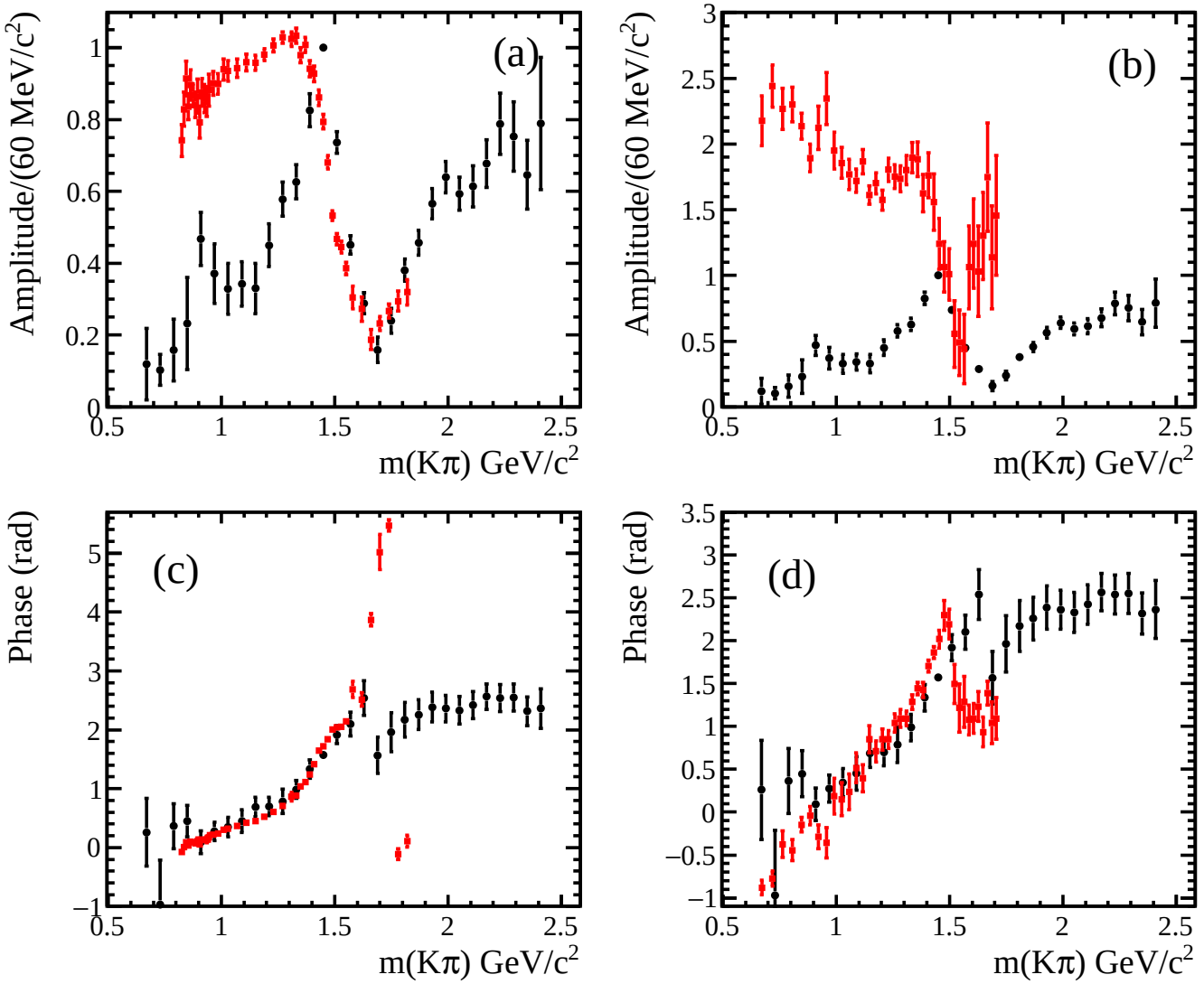

FIG. 14: The $I = 1/2$ $K\pi$ $\mathcal{S}$-wave amplitude measurements from $\eta_c \to K^0_S K^\pm \pi^\mp$ compared to the (a) LASS and (b) E791 results: the corresponding $I = 1/2$ $K\pi$ $\mathcal{S}$-wave phase measurements compared to the (c) LASS and (d) E791 measurements. Black dots indicate the results from the present analysis; square (red) points indicate the LASS or E791 results. The LASS data are plotted in the region having only one solution.

experiment at SLAC. We find that, in comparison with the isobar models examined here, an improved description of the data is obtained by using a MIPWA method.

We extract the $I = 1/2$ $K\pi$ $\mathcal{S}$-wave amplitude and phase and find good agreement between the measurements for the two η_c decay modes. The $K\pi$ $\mathcal{S}$-wave is dominated by the presence of the $K^*_0(1430)$ resonance which is observed as a clear peak with the corresponding increase in phase of about π expected for a resonance. A broad structure in the 1.95 GeV/c^2 mass region indicates the presence of the $K^*_0(1950)$ resonance.

A comparison between the present measurement and previous experiments indicates a similar trend for the phase up to a mass of 1.5 GeV/c^2. The amplitudes, on the other hand, show very marked differences.

To fit the data we need to introduce a new $a_0(1950)$ resonance in both $\eta_c \to K^0_S K^\pm \pi^\mp$ and $\eta_c \to K^+ K^- \pi^0$ decay modes, and their associated parameter values are in good agreement. The weighted averages for the parameter values are:

$$\begin{aligned} m(a_0(1950)) &= 1931 \pm 14 \pm 22 \text{ MeV}/c^2, \\ \Gamma(a_0(1950)) &= 271 \pm 22 \pm 29 \text{ MeV} \end{aligned} \quad (12)$$

with significances of 2.5σ and 4.2σ respectively, including systematic uncertainties. These results are, however, systematically limited, and more detailed studies of the $I = 1$ $K\overline{K}$ $\mathcal{S}$-wave will be required in order to improve

TABLE VI: Results from the $\eta_c \to K^0_S K^\pm \pi^\mp$ Dalitz plot analysis using an isobar model. The listed uncertainties are statistical only.

Amplitude	Fraction %	Phase (rad)
$K_0^*(1430)\overline{K}$	40.8 ± 2.2	0.
$K_0^*(1950)\overline{K}$	14.8 ± 1.7	-1.00 ± 0.07
NR	18.0 ± 2.5	1.94 ± 0.09
$a_0(980)\pi$	10.5 ± 1.2	0.94 ± 0.12
$a_0(1450)\pi$	1.7 ± 0.5	2.94 ± 0.13
$a_0(1950)\pi$	0.7 ± 0.2	-1.76 ± 0.24
$a_2(1320)\pi$	0.2 ± 0.2	-0.53 ± 0.42
$K_2^*(1430)\overline{K}$	2.3 ± 0.7	-1.55 ± 0.11
Total	88.8 ± 4.3	
$-2\log\mathcal{L}$	-4290.7	
$\chi^2/N_{\rm cells}$	467/256=1.82	

the precision of these values.

X. ACKNOWLEDGEMENTS

We are grateful for the extraordinary contributions of our PEP-II colleagues in achieving the excellent luminosity and machine conditions that have made this work possible. The success of this project also relies critically on the expertise and dedication of the computing organizations that support *BABAR*. The collaborating institutions wish to thank SLAC for its support and the kind hospitality extended to them. This work is supported by the US Department of Energy and National Science Foundation, the Natural Sciences and Engineering Research Council (Canada), the Commissariat à l'Energie Atomique and Institut National de Physique Nucléaire et de Physique des Particules (France), the Bundesministerium für Bildung und Forschung and Deutsche Forschungsgemeinschaft (Germany), the Istituto Nazionale di Fisica Nucleare (Italy), the Foundation for Fundamental Research on Matter (The Netherlands), the Research Council of Norway, the Ministry of Education and Science of the Russian Federation, Ministerio de Economia y Competitividad (Spain), and the Science and Technology Facilities Council (United Kingdom). Individuals have received support from the Marie-Curie IEF program (European Union), the A. P. Sloan Foundation (USA) and the Binational Science Foundation (USA-Israel). The work of A. Palano and M. R. Pennington was supported (in part) by the U.S. Department of Energy, Office of Science, Office of Nuclear Physics under contract DE-AC05-06OR23177.

[1] G.'t Hooft *et al.*, Phys. Lett. B **662**, 424 (2008); W. Ochs, J.Phys. G **40**, 043001 (2013).
[2] B. Aubert *et al.* (*BABAR* Collaboration), Phys. Rev. D **71**, 032005 (2005); B. Aubert *et al.* (*BABAR* Collaboration), Phys. Rev. D **78**, 034023 (2008); B. Aubert *et al.* (*BABAR* Collaboration), Phys. Rev. D **78**, 012004 (2008); A. Poluektov *et al.* (Belle Collaboration), Phys. Rev. D **81**, 112002 (2010).
[3] K. Chilikin *et al.* (Belle Collaboration), Phys. Rev. D **88**, 074026 (2013); R. Aaij *et al.* (LHCb Collaboration), Phys. Rev. Lett. **112**, 222002 (2014).
[4] R. Aaij *et al.* (LHCb Collaboration), Phys. Rev. D **90**, 072003 (2014).
[5] D. Aston *et al.* (LASS Collaboration), Nucl. Phys. B **296**, 493 (1988).
[6] B. Aubert *et al.* (*BABAR* Collaboration), Phys. Rev. D **79**, 112001 (2009).
[7] E. M. Aitala *et al.* (E791 Collaboration), Phys. Rev. Lett. **89**, 121801 (2002).
[8] E. M. Aitala *et al.* (E791 Collaboration), Phys. Rev. D **73**, 032004 (2006); Erratum-ibid. D **74**, 059901 (2006).
[9] G. Bonvicini *et al.* (CLEO Collaboration), Phys. Rev. D **78**, 052001 (2008).
[10] J. M. Link *et al.* (FOCUS Collaboration), Phys. Lett. B **653**, 1 (2007).
[11] B. Aubert *et al.* (*BABAR* Collaboration), Phys. Rev. D **79**, 032003 (2009).
[12] B. Aubert *et al.* (*BABAR* Collaboration), Phys. Rev. D **89**, 112004 (2014).
[13] P. del Amo Sanchez *et al.* (*BABAR* Collaboration), Phys. Rev. D **84**, 012004 (2011).
[14] C. N. Yang, Phys. Rev. **77**, 242 (1950).
[15] J. P. Lees *et al.* (*BABAR* Collaboration), Nucl. Instrum. Methods Phys. Res., Sect. A **726**, 203 (2013).
[16] B. Aubert *et al.* (*BABAR* Collaboration), Nucl. Instrum. Methods Phys. Res., Sect. A **479**, 1 (2002); *ibid.* **729**, 615 (2013).
[17] The *BABAR* detector Monte Carlo simulation is based on Geant4 [S. Agostinelli *et al.*, Nucl. Instrum. Methods A **506**, 250 (2003)] and EvtGen [D. J. Lange, Nucl. Instrum. Methods A **462**, 152 (2001)].
[18] B. Aubert *et al.* (*BABAR* Collaboration), Phys. Rev. D **81**, 092003 (2010).
[19] K. A. Olive *et al.* (Particle Data Group), Chin. Phys. C **38**, 090001 (2014).
[20] B. Aubert *et al.* (*BABAR* Collaboration), Phys. Rev. D **77**, 092002 (2008).
[21] The use of charge conjugate reactions is implied, where not explicitly expressed, throughout the paper.
[22] M. J. Oreglia, Ph.D. Thesis, SLAC-R-236 (1980); J. E. Gaiser, Ph.D. Thesis, SLAC-R-255 (1982); T. Skwarnicki, Ph.D. Thesis, DESY-F31-86-02 (1986).
[23] M. Ablikim *et al.* (BESIII Collaboration), Phys. Rev. Lett. **108**, 222002 (2012).
[24] S. Kopp *et al.* (CLEO Collaboration), Phys. Rev. D **63**, 092001 (2001).
[25] J. Blatt and V. Weisskopf, Theoretical Nuclear Physics, New York: John Wiley & Sons (1952).
[26] A. Abele *et al.* (Crystal Barrel Collaboration), Phys. Rev. D **57**, 3860 (1998).
[27] P. E. Condon and P. L. Cowell, Phys. Rev. D **9**, 2558 (1974).